Microstructural Evolution of Melt Intercalated Polymer−Organically Modified Layered Silicates Nanocomposites

Richard A. Vaia,† Klaus D. Jandt, Edward J. Kramer,* and Emmanuel P. Giannelis*

Department of Materials Science and Engineering and the Materials Science Center, Cornell University, Ithaca, New York 14853

Received February 6, 1996. Revised Manuscript Received June 24, 1996[⊗]

The microstructure of various (ordered and disordered) polymer−organically modified layered silicate hybrids, synthesized via static polymer melt intercalation, is examined with X-ray diffraction and transmission electron microscopy. The ordered intercalates exhibit microstructures very similar to the unintercalated organically modified layered silicate (OLS). Polymer intercalation occurs as a front which penetrates the primary OLS particle from the external edge. The disordered hybrids, on the other hand, exhibit heterogeneous microstructures with increased layer disorder and spacing toward the polymer−primary particle boundary. In these hybrids, individual silicate layers are observed near the edge, whereas small coherent layer packets separated by polymer-filled gaps are prevalent toward the interior of the primary particle. The heterogeneous microstructure indicates that the formation of these disordered hybrids occur by a more complex process than simple sequential separation of individual layers starting from the surface of the crystallites and primary particles. In general, the features of the local microstructure from TEM give useful detail to the overall picture that can be drawn from the XRD results and enhance the understanding of various thermodynamic and kinetic issues surrounding hybrid formation.

Introduction

Polymer melt intercalation is a promising new approach to fabricate polymer-layered silicate (PLS) nanocomposites using conventional polymer-processing techniques.[1−6] Hybrids are formed by heating a mixture of polymer and layered silicate above the glass transition or melting temperature of the polymer. The formation can be aided by shear (e.g., by mixing in an extruder), but will occur readily in the absence of shear.[3] The ultrafine phase dimensions of nanocomposites, typically ranging between 1 and 10 nm, lead to new and improved properties when compared to their pure polymer constituent or their macrocomposite counterparts.[7] For example, polymer−silicate nanocomposites exhibit increased modulus,[8−10] decreased thermal expansion coefficient,[9] reduced gas permeability,[9,11] increased solvent resistance,[6] and enhanced ionic conductivity[2] when compared to the pristine polymers. These performance improvements, though, depend greatly on the distribution, arrangement, and interfacial bonding between the silicate layers and the polymer.

The formation of PLS nanocomposites via polymer melt intercalation depends upon the thermodynamic interaction between the polymer and host silicate as well as transport of polymer chains from the bulk melt into the silicate interlayers. Previous studies indicate that the surface energy of the layered silicates and thus their interaction with polymer matrixes can be easily fine-tuned by judicious choice of the interlayer cation.[4,5] However, just as critical to hybrid formation is the transport of polymer chains into the silicate. The transport pathways and mechanisms depend on the morphology and nanostructure of the layered host. The layer size, spatial distribution, and defect structure will influence transport of polymer into the silicate interlayer, movement of the layers into the polymer bulk, and the potential number of favorable polymer−silicate interaction sites.

Previously we have used X-ray diffraction (XRD) to characterize the structure of the polymer−silicate hybrids[1,2,5,6] and study the kinetics of the polymer melt intercalation.[3] By monitoring the position, shape, and intensity of the basal reflections from the silicate layers, the hybrid structure (*intercalated* where extended polymer chains occupy the interlayer space between silicate layers or *exfoliated* where the silicate layers are dispersed in a continuous polymer matrix) may be identified.[5] Briefly, for *exfoliated* hybrids, the extensive layer separation associated with delamination of the original silicate structure in the polymer matrix results in the

† Current address: Polymer Branch, Materials Directorate, Wright Laboratory, Wright-Patterson AFB, Dayton, OH 45433.

⊗ Abstract published in *Advance ACS Abstracts,* September 1, 1996.

(1) Vaia, R. A.; Ishii, H.; Giannelis, E. P. *Chem. Mater.* **1993**, *5*, 1694.
(2) Vaia, R. A.; Vasudevan, S.; Krawiec, W.; Scanlon, L. G.; Giannelis, E. P. *Adv. Mater.* **1995**, *7*, 154.
(3) Vaia, R. A.; Jandt, K. D; Kramer, E. J.; Giannelis, E. P. *Macromolecules* **1995**, *28*, 8080.
(4) Vaia, R. A.; Giannelis, E. P., submitted to *Macromolecules.*
(5) Vaia, R. A.; Giannelis, E. P., submitted to *Macromolecules.*
(6) Burnside, S. D; Giannelis, E. P. *Chem. Mater.* **1995**, *7*, 1597.
(7) For recent review of nanocomposites, see: Komarneni, S. *J. Mater. Chem.* **1992**, *2*, 1219.
(8) Usuki, A.; et al. *J. Mater. Res.* **1993**, *8*, 1179.
(9) Yano, K.; Usuki, A.; Kurauchi, T.; Kamigaito, O. *J. Polym. Sci., Part A: Polym. Chem.* **1993**, *31*, 2493.
(10) Messersmith, P. B.; Giannelis, E. P. *Chem. Mater.* **1994**, *6*, 1719.
(11) Messersmith, P. B.; Giannelis, E. P. *J. Polym. Sci., Part A: Polym. Chem.* **1995**, *33*, 1047.

S0897-4756(96)00102-0 CCC: $12.00

eventual disappearance of any coherent X-ray scattering from the layers. On the other hand, for *intercalated* hybrids, the finite layer expansion associated with polymer intercalation results in the appearance of a new basal reflection corresponding to the larger gallery height. A relative increase or decrease in the degree of coherent stacking of the silicate layers due to *ordering* or *disordering* is reflected in a decrease or increase in the width (full width at half maximum, fwhm) of the basal reflections, respectively. In contrast, for immiscible mixtures, the original silicate structure is preserved, and thus the characteristics (position, height, and width) of the silicate basal reflection remain unchanged.

Although XRD allows for precise, routine measurements of silicate layer spacing (1−4 nm), little can be said about the spatial distribution of the silicate layers or any structural inhomogeneities in the hybrids. Additionally, some layered silicates do not initially exhibit well-defined basal reflections. Thus peak broadening and intensity decreases are difficult to follow systematically. Therefore, conclusions concerning mechanisms of hybrid formation and hybrid microstructure based solely on XRD results are only tentative.

In contrast to the global averaging of XRD, conventional transmission electron microscopy (TEM) and high-resolution transmission microscopy (HRTEM) can provide information in real space, in a localized area, on morphology, atomic arrangement, spatial distribution of the various phases, and defect structures. However, special care must be exercised to guarantee a representative cross section of the sample. TEM has been utilized over the past 30 years to study mica-type layered silicates and their mineralogical habits; however, it has only been used minimally in previous studies of melt intercalation.[3]

In this report we combine XRD and TEM to examine the microstructure of various polymer−OLS nanocomposites synthesized via static polymer melt intercalation.[12] When used in conjunction, XRD and TEM are complementary in that many issues not determinable by one are resolved when both techniques are utilized. Using TEM and HRTEM, we examine the microstructure of ordered intercalates at various stages of formation as well as the final microstructure of disordered hybrids. The observed microstructures are compared with those concluded from XRD results. With this increased understanding of the hybrid microstructure, various thermodynamic and kinetic issues surrounding hybrid formation are discussed.

Experimental Section

Synthesis. Organically modified layered silicates, F18 (octadecylammonium-exchanged fluorohectorite) and F12 (dodecylammonium-exchanged fluorohectorite), were synthesized, as previously outlined, by a cation-exchange reaction between Li fluorohectorite (Corning Inc.) and octadecylamine and dodecylamine (Aldrich), respectively.[13] The polymers utilized were polystyrene (PS) and poly(3-bromostyrene) (PS3Br). Table 1 summarizes the specifics of the hosts and polymers used.

Table 1. Characteristics of OLSs and Polymers

OLS	initial gallery height (nm)	no. of C atoms/ chain	area/chain (nm^2)	polymer	$\bar{M}_w$	$\bar{M}_w/\bar{M}_n$	T_g, °C
F18	1.2	18	0.39	PS30	30 000	1.06	96
F12	0.9	12	0.39	PS400	400 000	1.06	100
				PS3Br	55 000	2.00	113

Hybrids were synthesized using the following procedure. Organically modified layered silicate (OLS) and polymer were mechanically mixed and formed into a pellet (25 $mm^2 \times 5$ mm) using a hydraulic press and a pressure of 70 MPa. Excess polymer (polymer:OLS ratio ~3:1 by weight) was used to avoid polymer depletion during melt intercalation. The pellets were subsequently annealed in vacuum at temperatures greater than the glass transition temperature of the polymer. For TEM investigations of partially intercalated hybrids, it was necessary to use the highest molecular weight polystyrene (PS400) and a larger polystyrene:F18 ratio (5:1) to achieve uniform ultrathin sections. Previous investigations have shown that the molecular weight of the polymer only affects the rate of polymer intercalation but not the final layer spacing of the hybrid.[1,3−5]

X-ray Diffraction. Room-temperature X-ray diffraction spectra were collected on a Scintag Inc. Θ−Θ diffractometer equipped with an intrinsic germanium detector system using Cu Kα radiation. In situ X-ray spectra of polystyrene melt intercalation were collected as outlined previously, by holding the sample in vacuum on a Pt60−Rh40 heating strip in a Buehler temperature controlled furnace attachment with beryllium windows for a Θ−Θ X-ray diffractometer.[3]

Transmission Electron Microscopy. Two sample-preparation procedures were used depending on the extent of the melt intercalation reaction. For fully intercalated samples, powders of the polymer−OLS hybrid were embedded in "Spurr" epoxy[14] and cured at 80 °C for 12 h. For partially intercalated PS400−F18 hybrid, the pellet was positioned in partially cured (70 °C for 45 min) "Spurr" epoxy such that a portion of the pellet was extending above the epoxy surface. The epoxy was then completely cured at 80 °C for 12 h. Partially cured epoxy was used to avoid epoxy intercalation in the unintercalated portion of the OLS.[15,16] XRD analysis of the resulting blocks verified that the epoxy mounting did not alter the structure of the partially intercalated or fully intercalated hybrids.

The epoxy block with the embedded powders of fully intercalated hybrid and the extruding portion of the partially intercalated hybrid pellet were cut to form a triangular block face (approximately 1 mm × 0.5 mm) for microtoming. Ultrathin sections (100 nm or less) were microtomed from this face, at room temperature, using a Reichert ultramicrotome. A water-filled boat was attached to the knife, so that after cutting, the ultrathin sections could be floated onto water. The sections were collected on gold TEM grids (hexagonal 400 mesh) and dried completely on filter paper at room temperature.

Microscopic investigations were performed on a JEOL 1200 EX TEM operating at 120 kV. Extra precautions were taken to minimize sample motion and beam damage of the epoxy, polystyrene, and silicate.[16−19] The TEM grids were mounted in a liquid nitrogen cooled sample holder and the brightness

(12) Throughout this paper, we will use the terminology proposed in our previous work[3] to describe the microstructural features of the OLSs. The silicate nominal particle (*agglomerate*) is comprised of an agglomeration of smaller oblong-shaped particles, referred to as *primary particles*. The primary particles consist of a compact face-to-face stacking or low-angle intergrowth of individual silicate *crystallites* (also known as tactoids). The crystallites consist of a coherent stacking of individual *silicate layers*.

(13) Vaia, R. A.; Teukolsky, R. K.; Giannelis, E. P., *Chem. Mater.* **1994**, *6*, 1017.
(14) Spurr, A. R. *Ultrastruct. Res.* **1969**, *26*, 31.
(15) Uncured Spurr epoxy and acrylic-based embedding formulations have been observed during embedding to intercalated OLS. Similar observations were reported in ref 16.
(16) Vali, H.; Köster, H. M. *Clay Miner.* **1986**, *21*, 827.
(17) Vali, H.; Hesse, R. *Am. Miner.* **1990**, *75*, 1443.
(18) Marcks, C. H.; Waschsmuth, H.; Reichenbach, H. G. V. *Clay Miner.* **1989**, *24*, 23.
(19) Klimentidis, R. E.; Mackinnon, I. D. R. *Clays Clay Miner.* **1986**, *34*, 155.

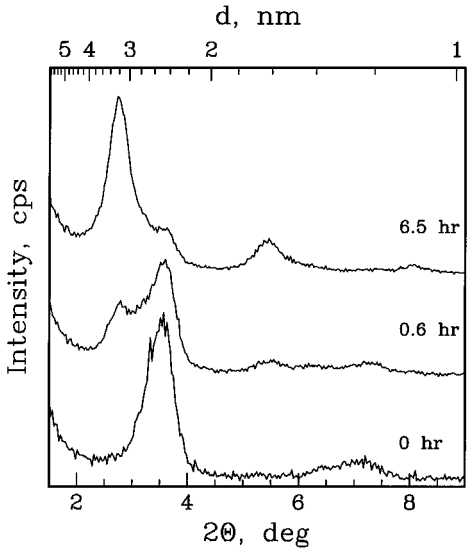

Figure 1. Temporal series (0, 0.6, and 6.5 h) of X-ray diffraction patterns for a PS30/F18 mixture annealed in situ at 155 °C. The breadth and intensity of the intercalated and unintercalated basal reflections are similar, representative of an ordered intercalate. At the beginning, the basal reflections characteristic of the unintercalated silicate structure (2θ = 4.15, 8.03; $d_{(001)}^{F18}$ = 2.13 nm) only are present. During the anneal, the intensity of the diffraction peaks corresponding to the unintercalated silicate is progressively reduced while a set of new peaks appear corresponding to the basal spacing of the PS30/F18 intercalated hybrid (2θ = 2.82, 5.66, 8.07; $d_{(001)}^{PS30/F18}$ = 3.13 nm).

of the electron beam was minimized (low-dose mode). Even with these precautions, the contrast of an area under investigation began to fade after a few minutes of beam exposure. This fading is attributed to destruction of the structure of the silicate layers and possible expulsion of interlayer organics by the electron beam.[16−19] All images were taken before contrast loss was visibly noticeable.

The scattering contrast in the bright-field mode of the TEM leads to "lattice fringes" corresponding to a periodic stacking sequence of silicate layers. Since the silicate layers are comprised of heavier elements (Al, Si, O) than the interlayer and surrounding matrix (C, H, N), they appear darker in bright field images.[19−22] The observed "lattice fringes" correspond to layer sequences that are tilted ±1° with respect to the electron beam axis (and the normal to the sample surface). For the sample thickness, projection of layer sequences with tilt greater than ±1° will result in overlap of individual layers and elimination of the fringes. Gallery height and layer spacing were determined by averaging at least 25 measurements of "lattice fringes" at 150 000 magnification. The magnification of the TEM was calibrated using the lattice fringe resolution of different standard TEM calibration samples. The error in measured gallery heights was estimated to be ±5%.

Results and Discussion

Ordered Intercalated Hybrids. Because of the lamellar structure of the ordered intercalate, XRD is a powerful technique to monitor the formation and structure of these hybrids. Figure 1 shows a temporal series (0, 0.6, and 6.5 h) of X-ray diffraction patterns for a PS30/F18 mixture annealed in situ at 155 °C. The width of the intercalated and unintercalated basal reflections is similar, representative of an ordered intercalate. At the beginning, only basal reflections characteristic of the unintercalated silicate structure ($d_{(001)}^{F18}$ = 2.13 nm) are present. During the anneal, the intensity of the diffraction peaks corresponding to the unintercalated silicate is progressively reduced while a set of new peaks appear corresponding to the basal spacing of the PS30/F18 intercalated hybrid ($d_{(001)}^{PS30/F18}$ = 3.13 nm). The fraction, χ, of F18 intercalated at a given time may be determined from the ratio of the integrated intensity of the intercalated and unintercalated (001) reflections.[3] At 0, 0.6, and 6.5 h, χ = 0.0, 0.3, and 0.7, respectively.

The width of the peaks, B (measured by the full width at half maximum), is inversely proportional to the coherence length of scattering entities and therefore reflects the coherent order of the silicate layers.[23] As the angular width of the reflection increases, the length over which coherency exists decreases. Initially, the breadth of the (001) reflection from the intercalated F18 is slightly greater (+20%) than that from the unintercalated F18, indicating that during the initial stages of polymer intercalation, the coherency of the intercalated silicate layers is slightly less than that of the original unintercalated F18. As the anneal progresses, the width of the new (001) reflection decreases toward that of the original unintercalated F18 becoming approximately equal between χ = 0.2 and 0.4. The width of the intercalated reflection then remain constant up to full intercalation (χ = 1).[26] Thus, we conclude on the basis of the XRD studies that polystyrene melt intercalation does not drastically alter the coherence length or disrupt the layer structure of the silicate crystallites. The morphology of the crystallites in the ordered intercalate (with the exception of a larger gallery height) should be the same as the original unintercalated F18.

To further investigate the microstructure of the ordered intercalate, verify the conclusions from XRD, and examine possible routes for polymer transport into the interlayer, a partially intercalated PS400/F18 hybrid (χ = 0.4; $B_{intercalated} = B_{unintercalated}$ = 0.0095 rad) was examined by transmission electron microscopy (TEM). Since the increased basal spacing associated with hybrid formation arises from the expansion of the interlayer to accommodate the intercalating polymer, regions of intercalated and unintercalated galleries should be distinguishable within the primary particle as regions with different layer spacing.

Figure 2 is a TEM bright field image of a portion of a F18 primary particle[12] surrounded by a matrix of polystyrene (light regions). Individual crystallites of F18 are visible as regions of alternating narrow, dark and light bands within the particle (fringes). On aver-

(20) Grim, R. E., *Clay Mineralogy*; McGraw-Hill: New York, 1953.
(21) Pinnavaia, T. J. In: *Chemical Physics of Intercalation*; Legrand, A. P., Flandrois, S., Eds.; Plenum: New York, 1987.
(22) Güven, N. In *Hydrous Phyllosilicates*; Bailey, S. W., Ed.; Mineralogical Society of America, Washington, DC, 1988; Reviews in Mineralogy, Vol. 19, pp 497−560.

(23) The breadth of the peaks, B (expressed as radians), is proportional to the coherence length of scattering entities, t, by the Scherrer relation, $B = A\lambda/t\cos(\theta)$, where A is a numerical proportionality constant.[24,25] We assume the contribution to peak width due to instrumental broadening is constant for 2θ = 2−4°.
(24) Dritis, V. A.; Tchoubar, C. *X-ray Diffraction by Disordered Lamellar Structures*; Springer-Verlag: New York, 1990; pp 21−22.
(25) Cullity, B. D. *Principles of X-ray Diffraction*; Addison-Wesley: Reading, MA, 1978.
(26) The behavior of the basal reflections in Figure 1 is representative of polystyrene melt intercalation of F18 at different temperatures and molecular weights as depicted in ref 3. In general, the initial intercalated basal reflection is 10−30% wider than the unintercalated reflection, and its breadth is within 5−10% of the original unintercalated reflection by $\chi \sim 0.2-0.4$.

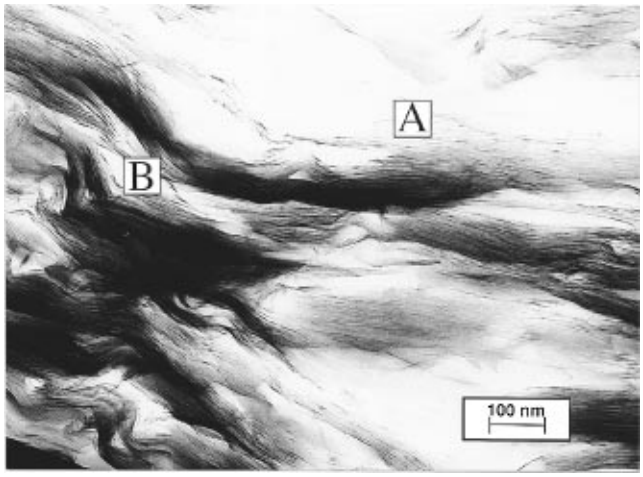

Figure 2. TEM bright-field image of a portion of a primary F18 particle (darker region) surrounded by a matrix of polystyrene (light region) in the ordered PS30/F18 intercalate. Compact face-to-face staking (A) or low-angle intergrowth (B) of crystallites are observable.

age, these crystallites are tightly packed and oriented along the major axis of the primary particle. Compact face-to-face stacking (two crystallites stacked with faces parallel, separated by less than 2−3 nm) or low-angle intergrowth (two crystallites converging at an acute angle into a single crystallite) of crystallites are observable.[16−20] Because of the tight packing of crystallites, the intercrystallite volume is generally small. The close crystallite packing produces slits between the crystallites that are typically only slightly greater than the height of the galleries within the crystallites.

The F18 crystallites consist of stacks of typically between 50 and 100 parallel silicate layers with lateral dimensions nominally between 0.05 and 0.5 μm (dark bands). The silicate layers are separated by galleries (light bands) containing in this case octadecylammonium cations with or without polystyrene. The extent of coherent stacking indicated by the number of parallel silicate layers (50−100 nm) is much greater than that determined from the breadth of the XRD basal reflection (∼15 nm).[23] This inconsistency indicates that the layer stacks observed in TEM contain defect structures that introduce fluctuations in interlayer spacing.

Bright-field TEM images of unintercalated crystallites located within the interior of a primary F18 particle are shown in Figures 3 and 4. Unintercalated crystallites are more prevalent towards the interior of the primary particle than near the primary particle−polymer boundary. The images show silicate layers with a 2.3 nm basal repeat distance, in agreement with XRD measurements. Irregularities in the intensity and contrast of the layers are attributed to beam damage and variations in the sample thickness. The repeat distance is comprised of ∼1.0 nm dark bands, corresponding to the silicate layers, separated by ∼1.3 nm light bands, corresponding to the octadecylammonium-containing galleries. In many instances, the crystallites and silicate layers exhibit substantial flexibility, bending locally by more than 30° while maintaining a fairly constant spacing. Generally, no subdetail within the silicate layer or gallery could be observed.

As anticipated, structural defects in the crystallite and irregularities in the layer stacking are commonly observed. In Figure 4, a higher magnification image of

Figure 3. Bright-field TEM image of unintercalated crystallites located within the interior of a primary particle in the ordered PS30/F18 intercalate.

an unintercalated crystallite shows local fluctuations in the layer spacing up to 2.5 nm (A). The fluctuations originate in the interlayer (light regions). Also observable within the crystallite are sites of layer termination (B) and layer division (C). These stacking defects cause the length of coherent X-ray scattering perpendicular to the layers to be less than the height of the crystallites. Additionally, these defects may play a vital role in polymer transport into the silicate interlayer by introducing additional transport paths, decreasing adhesion between the layers, and increasing the effective flexibility of the silicate layers.

Figure 5 shows a bright-field TEM micrograph of a PS intercalated crystallite near the edge of a primary particle. In contrast to the unintercalated crystallites, the intercalated crystallites are more prevalent near the primary particle−polymer boundary. Layer spacings correspond to a 2.9 ± 0.1 nm basal repeat distance. The larger repeat distance arises from increases in the gallery height (light regions) due to polymer intercalation. The slightly smaller value compared to XRD (3.1 nm) may be due to radiation damage of the interlayer organics under the electron beam.[15] Aside from layer expansion, the intercalated crystallites display the same features observed in the unintercalated crystallite—local fluctuations in layer spacing, layer termination, and structural irregularities. No crystallites were observed that contained both intercalated and unintercalated layers.

In both intercalated and unintercalated crystallites, the extent of layer stacking (size of the coherent units) is similar. Even at the polymer−primary particle boundary where silicate layers terminate in the polymer matrix, the coherency of layer stacking is generally preserved, and the intercalated layer height is the same as observed further within the primary particle. Figure 6 shows a small layer stack terminating in the polystyrene matrix. The layers are equally spaced (3.0 nm) up to the edge of the crystallite. The polystyrene is in intimate contact with the crystallite and shows substantial penetration into the primary particle through

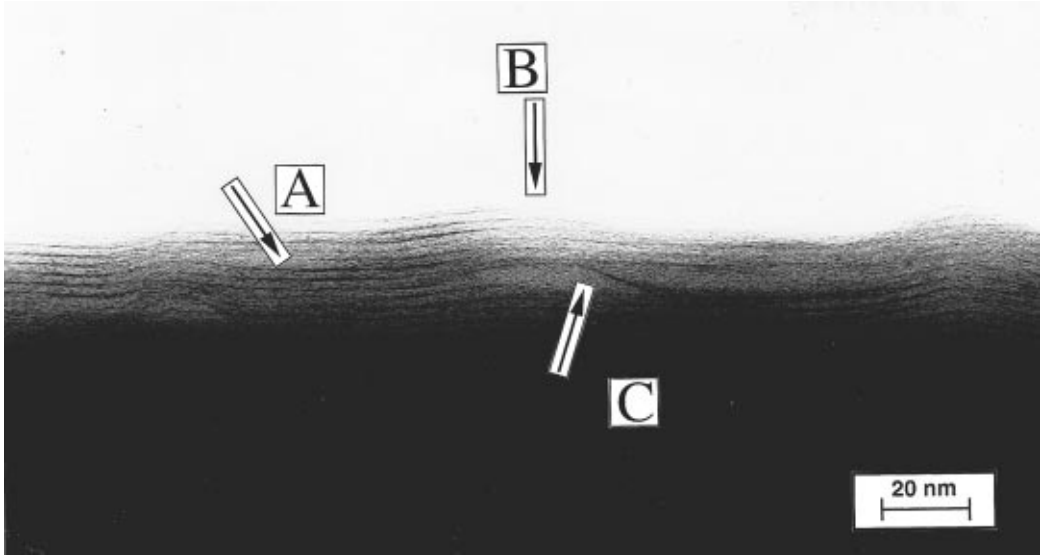

Figure 4. High-resolution bright-field TEM image of a portion near an unintercalated crystallite located within the interior of a primary particle in the ordered PS30/F18 intercalate. Local fluctuations in the layer spacing up to 2.5 nm (A), sites of layer termination (B), and layer division (C) are observable. The white region at the top of the image is a crack in the TEM ultrathin section.

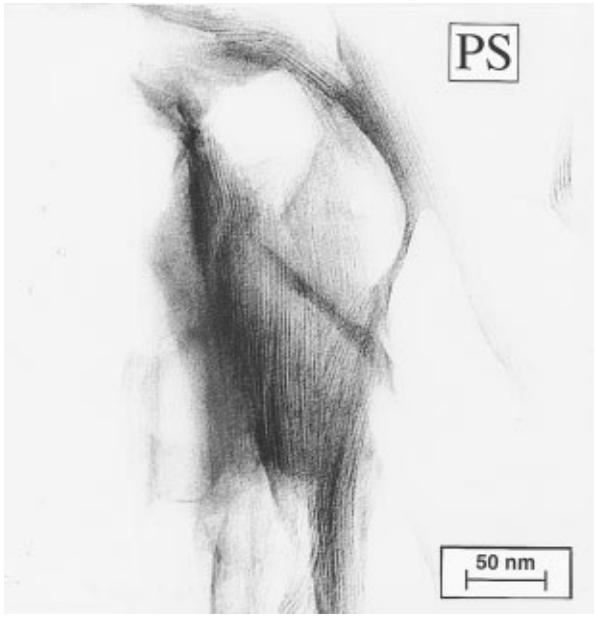

Figure 5. Bright-field TEM image of an intercalated crystallite near the edge of a primary particle in the ordered PS30/F18 intercalate showing termination of silicate layers in the polystyrene matrix (A).

areas between the crystallites. The similar microstructure of the intercalated and unintercalated crystallites corroborates the similarity in the fwhm of the (001) basal reflections.

For the sample examined in the above micrographs, approximately 40% of the silicate interlayers contain polystyrene. From the relative location and local morphology of these regions, conclusions about possible routes for hybrid formation can be deduced. Since the silicate layers are impenetrable in the direction perpendicular to their long axis, polystyrene must intercalate the gallery from the edges of the crystallites. For polymer to reach the crystallite edge, the melt must first penetrate the primary particles. Thus, on the scale of the primary particle, two pathways are possible for polymer transport into the primary particle. Either polymer intercalation takes place uniformly throughout

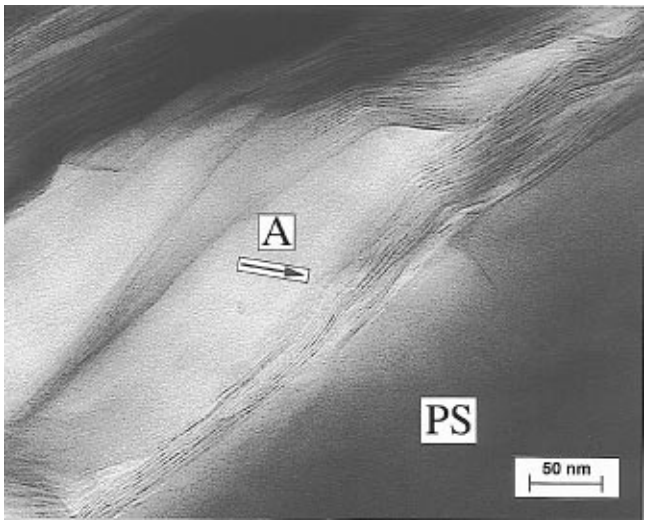

Figure 6. High-resolution bright-field TEM image of an intercalated primary particle near the polystyrene matrix in the ordered PS30/F18 intercalate.

the primary particle or as a front penetrating the primary particle from the exterior. If hybrid formation occurred uniformly throughout the primary particle, the distribution of intercalated and unintercalated regions within the primary particle should be uniform and a substantial number of crystallites should contain both intercalated and unintercalated regions. However, the predominance of intercalated crystallites at the exterior of the primary particle and the absence of crystallites containing both intercalated and unintercalated regions imply the second mechanism is more likely in polystyrene intercalation. These observations also agree with the conclusions of the kinetic studies described earlier.[3]

Disordered Hybrids. In contrast to the ordered intercalates, disordered hybrids do not produce well-defined basal reflections in XRD. Figure 7 compares the X-ray diffraction patterns of PS30/F12 and PS3Br/F12 hybrid. Both hybrids contain 20 vol % F12. The diffraction pattern of unintercalated F12, annealed at the same temperature, is included for comparison. The PS30/F12 hybrid represents a disordered intercalate.

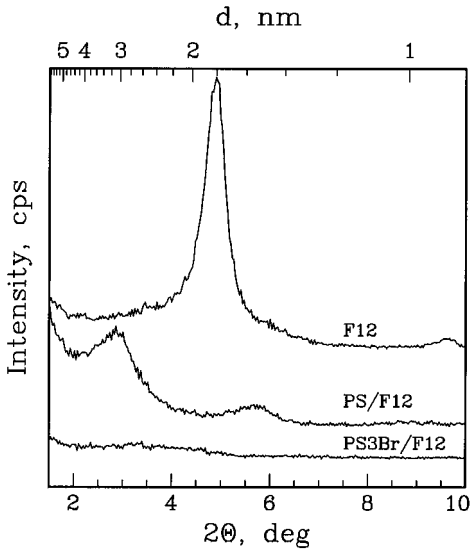

Figure 7. X-ray diffraction patterns of PS30/F12 and PS3Br/F12 hybrid. Both hybrids contain 20 vol % F12. These spectra are representative of disordered hybrids. The diffraction pattern of unintercalated F12 is included for comparison.

The basal reflections ($2\theta = 3.0°, 5.5°$) correspond to an increased gallery height. The d spacing for F12 and PS30/F12 is 1.8 and 2.9 nm, respectively. However, the intercalated reflections are substantially broader than those of the unintercalated F12 ($B^{PS30/F12} = 0.021$ rad and $B^{F12} = 0.009$ rad). In contrast to PS30/F12, PS3Br/F12 represents an exfoliated hybrid. The X-ray diffraction pattern is almost featureless, only exhibiting a very broad, extremely weak reflection at approximately $2\theta = 3.75°$.

In general, many factors other than layer disorder, such as intercalate composition, sample geometry, layer spacing greater than 4−5 nm, and silicate concentration may contribute to a decreased intensity of the basal reflection or a featureless diffraction pattern. For example, it is theoretically possible that the weak basal intensity from the PS3Br/F12 hybrid could be a result of the large X-ray absorption factor of bromine relative to carbon and hydrogen as well as from delamination of the silicate layers. Thus, it is difficult to draw definitive conclusions about the structure of the hybrids exhibiting relatively featureless diffraction patterns. Only general conclusions about layer order and layer spacing can be inferred. In such cases, TEM is necessary to determine the nature of the hybrids and provide additional information that will aid in the interpretation of the XRD results.

Figure 8 is a bright-field TEM image of a fully intercalated PS30/F12 hybrid with comparable magnification to the image of PS400/F18 in Figure 2. Penetration of polystyrene into the primary F12 particle disrupts the original crystallite structure to a greater extent than observed with PS400/F18. Layer spacings range from 2.1 to 6.0 nm. Near the polymer−primary particle interface, areas between layer stacks containing polystyrene (indicated by the arrows) are observable with widths approaching 5−6 nm. From a series of higher magnification images, the mean layer spacing toward the interior of the crystallites is approximately 2.8 nm. On average, coherent stacking of 10−20 layers is seen compared to an average stack of about 50−100 layers for PS400/F18. Note that the extent of coherent

Figure 8. Bright-field TEM image of a fully intercalated PS30/F12 hybrid with magnification comparable to the image of PS400/F18 in Figure 2. Arrows indicate areas with layer spacing ~5 nm.

stacking observed in TEM (10−20 nm) is greater than that determined from the breadth of the basal reflection (7 nm), indicating that defects in layer stacking are probably present in the PS/F12 hybrids as they were in the PS400/F18 hybrids.

Figure 8 also shows that the microstructure of the primary F12 particles is heterogeneous. Regions of coherent order are more prevalent toward the interior of the primary particles than near the polymer−primary particle interface. The increase in layer order away from the polymer−primary particle interface may result from kinetic factors associated with the relative rates of volume expansion of the primary particle into the surrounding polystyrene matrix and of polymer intercalation of the interior crystallites. The features of the local microstructure from TEM give useful detail to the overall picture that can be drawn from the XRD results.

Figure 9 is a bright-field TEM image of the PS3Br/F12 hybrid with comparable magnification to the images in Figure 2 and 8. Even though the XRD pattern is featureless, some layer order is readily observable and the location and structure of the original crystallites and the primary particle are still discernible. It is believed that the brominated polystyrene is more strongly attracted to the silicate surface (modified by the alkylammonium cations) than is polystyrene.[5] The large gallery heights and disordered structure observed even without shear are consistent with this belief and agree with predictions we made earlier using a mean-field thermodynamic model for polymer melt intercalation.[4] The TEM results also indicate that such hybrids can be thermodynamically stable and do not require special approaches or external inputs of energy to form.

Figures 10 and 11 are high-resolution bright-field images at the PS3Br−primary F12 particle boundary and near the interior of a primary F12 particle, respectively. As observed for the PS30/F12 hybrids, the extent of coherent layer stacking in the PS3Br/F12 hybrid increases toward the interior of the primary F12 par-

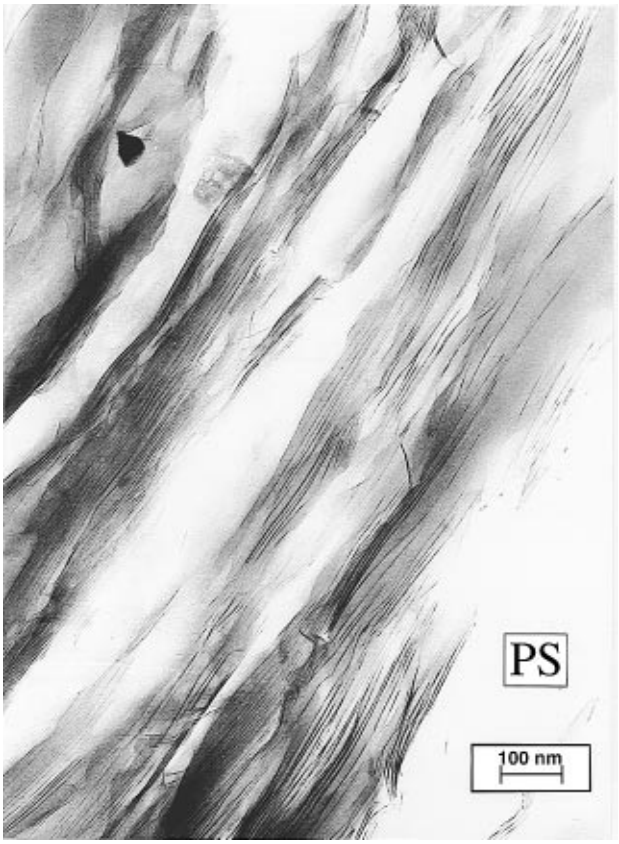

Figure 9. Bright-field TEM image of the PS3Br/F12 hybrid with magnification comparable to the images in Figures 2 and 8.

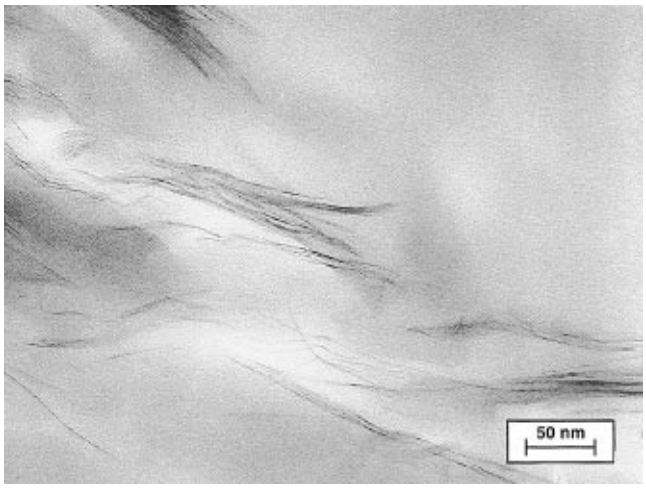

Figure 10. High-resolution bright-field TEM image of crystallite and silicate layers at the PS3Br−primary F12 particle boundary in the PS3Br/F12 hybrid.

ticle. However, PS3Br penetration of the primary particle occurs to a much greater extent than PS30.

Figure 10 shows individual silicate layers dispersed in the polymer matrix. The thickness of the dark lines (~1.0 nm) correspond well with the known crystallographic thickness of an individual silicate layer (0.96 nm).[7−9] The effect of the extremely large aspect ratio of the layers (100−1000) on the relative layer order is demonstrated in the preferential alignment of the layers even at these large separations (>10 nm). Additionally, the flexibility of the layers is clearly demonstrated. Even though the layers are "ceramic" in nature, because of their very large aspect ratio and nanometer thickness,

Figure 11. High-resolution bright-field image of crystallite and silicate layers near the interior of a primary F12 particle in the PS3Br/F12 hybrid.

they behave mechanically more like stacks of paper than rigid plates.

From Figure 11, extensive polymer penetration into the galleries is apparent, and intercrystallite gaps up to 5−20 nm are observed within the interior of the primary particle. These large spacings separate coherent layer stacks of 5−20 layers with interlayer spacings between 2 and 4 nm. The F12 crystallites near the interior appear to preferentially separate into small coherent stacks instead of delaminating layer-by-layer as seen near the edge of the primary particle.

The heterogeneity of the layer groupings in the primary particle implies that the formation of these disordered hybrids occur by a more complex process than simple sequential separation of individual layers starting from the surface of the primary particle and crystallite as previously proposed for small molecule intercalation of layered materials.[27−29] The galleries and intercrystallite gaps which expand and separate the original crystallites may contain defect structures or local chemical inhomogeneities that facilitate polymer transport or result in enhanced polymer−silicate interaction, respectively. Longer range forces such as electrostatics or stress fields associated with gallery expansion and layer bending will, depending on the local surroundings and location within the original primary particle, act to maintain layer groupings of an optimal size. Delamination of the crystallite structure probably occurs layer-by-layer near the edge of the primary particle but steric and/or electrostatic factors within the interior of the primary particle inhibit layer-by-layer separation and thus polymer transport via intercrystalline gaps and defect regions dominates. We are currently investigating the mechanisms of delamination more closely.

The effect of aliphatic chain length and the chemical nature of the polymer on hybrid microstructure is

(27) Schöllhorn, R. *Physica* **1980**, *99B*, 89.
(28) Parry, G. S. *Physica* **1981**, *105B*, 261.
(29) Lagaly, G. *Philos. Trans. R. Soc. London A* **1984**, *311*, 315.

consistent with tentative predictions from a mean-field thermodynamic treatment of the melt intercalation process.[4−5] In the simplest sense, the entropic penalty associated with polymer confinement may be compensated by an entropic gain associated with layer separation and the increased conformational freedom of the interlayer aliphatic chains. Therefore, the interlayer structure, which depends on the length of the aliphatic chains, should be optimized to maximize the conformational freedom of the chains upon intercalation and facilitate favorable polymer−silicate interactions. In addition, polar polymers containing groups capable of associative interactions with the host surface are preferred. Thus, the increased polarity of the PS3Br (with respect to PS) will interact more favorably with the polar fluorohectorite interlayer surface, resulting in a more disordered hybrid as experimentally observed. As a corollary to these results, the increased polymer−OLS interaction should increase the frictional coefficient associated with polymer transport within the interlayer and result in slower melt intercalation kinetics. Qualitatively, we have experimentally observed these effects.

The heterogeneous structure of these hybrids demonstrates the kinetic limits of static processing. For static processing, layer homogenization depends on Brownian motion of the silicate layers in the polymer melt. Because of the large lateral dimensions of the layers ($\sim$1 μm) and the high intrinsic viscosity of the polymer melt, mass transport of the layers via Brownian motion is prohibitively slow. Recent results indicate that shear processing, such as with an ultrasonicator, parallel plate rheometer, or conventional compounding equipment, facilitates silicate layer−polymer mixing and increases the uniformity of layer distribution in the polymer matrix.[6,30]

(30) Krishnamoorti, R.; Giannelis, E. P., submitted to *Macromolecules*.

Conclusions

TEM investigations of the polymer−silicate nanocomposites confirm and complement our previous results from XRD. The ordered intercalates exhibit microstructures very similar to the unintercalated OLS. Polymer intercalation occurs as a front which penetrates the primary OLS particle from the external edge. The disordered hybrids exhibit heterogeneous microstructures with increased layer disorder and spacing towards the polymer−primary particle boundary. In these hybrids, individual silicate layers are observed near the edge whereas small coherent layer packets separated by polymer-filled gaps are prevalent toward the interior of the primary particle. The heterogeneous microstructure indicates that the formation of these disordered hybrids occurs by a more complex process than simple sequential separation of individual layers starting from the surface of the crystallites and primary particles. In general, the features of the local microstructure from TEM give useful detail to the overall picture that can be drawn from the XRD results and enhance the understanding of various thermodynamic and kinetic issues surrounding hybrid formation.

Acknowledgment. Primary support of this work came from the Materials Science Center (MSC) at Cornell University (funded by NSF-DMR-MRSEC) and its Polymer Outreach Program through grants from Corning, Inc. and by generous gifts from Amcol, Dow, DuPont, Exxon, Hercules, Monsanto, Southern Clay Products, and Xerox. R.A.V. gratefully acknowledges the financial support of a NDSEG Fellowship. K.D.J. is grateful for the partial financial support of a Feodor-Lynen Fellowship of the Alexander von Humboldt Foundation, Bonn, Germany. We wish to thank C. Daugherty, N. Rizzo, J. Hunt, and I. Karr for their assistance. This study benefited from the use of the Central Facilities of the MSC.

CM960102H